

# No influence of passing stars on paleoclimate reconstructions over the past 56 million years

RICHARD E. ZEEBE<sup>1</sup> AND DAVID M. HERNANDEZ<sup>2</sup>

<sup>1</sup> *SOEST, University of Hawaii at Manoa, 1000 Pope Road, MSB 629, Honolulu, HI 96822, USA.* <sup>a</sup> <sup>b</sup>

<sup>2</sup> *Department of Astronomy, Yale University, Kline Biology Tower, 219 Prospect St, New Haven, CT 06511, USA.* <sup>c</sup>

Final Accepted Version, *The Astronomical Journal*

## ABSTRACT

Passing stars (also called stellar flybys) have notable effects on the solar system’s long-term dynamical evolution, injection of Oort cloud comets into the solar system, properties of trans-Neptunian objects, and more. Based on a simplified solar system model, omitting the Moon and the Sun’s quadrupole moment  $J_2$ , it has recently been suggested that passing stars are also an important driver of paleoclimate before  $\sim 50$  Myr ago, including a climate event called the Paleocene-Eocene Thermal Maximum ( $\sim 56$  Myr ago). In contrast, using a state-of-the-art solar system model, including a lunar contribution and  $J_2$ , and random stellar parameters ( $>400$  simulations), we find no influence of passing stars on paleoclimate reconstructions over the past 56 Myr. Even in an extreme flyby scenario in which the Sun-like star HD 7977 ( $m = 1.07 M_\odot$ ) would have passed within  $\sim 3,900$  au about 2.8 Myr ago (with 5% likelihood), we detect no discernible change in Earth’s orbital evolution over the past 70 Myr, compared to our standard model. Our results indicate that a complete physics model is essential to accurately study the effects of stellar flybys on Earth’s orbital evolution.

*Keywords:* Solar System (1528) Orbits (1184) Celestial mechanics (211) Solar neighborhood (1509)

## 1. INTRODUCTION

Gravitational interactions due to stellar flybys have a variety of effects on the solar system, including its long-term dynamical evolution, injection of Oort cloud comets into the solar system, properties of trans-Neptunian objects, etc. (e.g., Oort 1950; Rickman 1976; Laughlin & Adams 2000; Malmberg et al. 2011; Li & Adams 2015; Batygin et al. 2020; Zink et al. 2020; Brown & Rein 2022; Pfalzner et al. 2024). However, the vast majority of flybys are weak and the likelihood of a strong flyby is small, even over the solar system’s lifetime. Based on Gaia Data Release 3 (Gaia DR3), Bailer-Jones (2022) estimated that the K7 dwarf Gl 710 ( $m = 0.7 M_\odot$ ) remains the closest known (future) encounter, with a median encounter distance of  $\sim 13,100$  au = 0.0636 pc, to occur in about 1.3 Myr. The second closest encounter was estimated to have occurred  $\sim 2.8$  Myr ago with the G3 dwarf HD 7977

( $m = 1.07 M_\odot$ ) and a median encounter distance of  $\sim 13,200$  au = 0.0641 pc (for more information on HD 7977, see, e.g., de la Fuente Marcos & de la Fuente Marcos 2022; Bobylev & Bajkova 2022; Dybczyński et al. 2024; Potemine 2024). Because most flybys are weak, the immediate consequences for, e.g, the planetary orbits are small or negligible. However, because of the solar system’s chaotic dynamics, small perturbations may have large-scale consequences in the long run (e.g., Zink et al. 2020; Brown & Rein 2022; Kaib & Raymond 2024).

The key question is, what is the relationship between the magnitude of the flyby perturbation and the magnitude of change in planetary orbits over a specified timescale (here  $\mathcal{O}(10^8$  y)). For instance, Kaib & Raymond (2024) suggested that a flyby scenario in which the star HD 7977 would have passed 2.8 Myr ago within only  $\sim 3,900$  au (5% likelihood, see Bailer-Jones 2022), would represent an important driver of paleoclimate before  $\sim 50$  Myr ago (for a discussion of causality, see Section 1.1). In other words, the magnitude of change in planetary orbits (in this case Earth’s orbital eccentricity) in response to such a perturbation would become significant over  $\sim 50$  Myr. It should be pointed out that in addition to primary gravitational interactions,

<sup>a</sup> Corresponding author: Richard E. Zeebe

<sup>b</sup> zeebe@soest.hawaii.edu

<sup>c</sup> david.m.hernandez@yale.edu

the most accurate state-of-the-art solar system models already include important secondary effects due to general relativity, the influence of the Moon (lunar contribution), the Sun’s quadrupole moment  $J_2$ , and asteroids (e.g., Laskar et al. 2011; Zeebe 2017, 2023a). Reliable predictions of orbital parameters based on these state-of-the-art models is limited to  $\sim 50$  Myr (without geological constraints) due to the solar system’s chaotic behavior. So should stellar flybys be added to accurate solar system models as an important secondary effect in multi-million year integrations?

**Table 1.** Selected variables and notation.

Variable	Unit	Meaning	Frame <sup>a</sup>	Note
$\mathbf{v}$	km s <sup>-1</sup>	Stellar velocity vector	LSR	$[v_1 \ v_2 \ v_3]$
$v$	km s <sup>-1</sup>	Stellar speed		$v =  \mathbf{v} $
$\sigma$	km s <sup>-1</sup>	Stellar velocity dispersion		<sup>b</sup>
$\mathbf{v}_\odot$	km s <sup>-1</sup>	Sun’s peculiar velocity	LSR	<sup>c</sup>
$\mathbf{X}_i$	au	Position solar system body $i$	ICS	
$\mathbf{V}_i$	au d <sup>-1</sup>	Velocity solar system body $i$	ICS	

<sup>a</sup>Reference frame (coordinate system): LSR = Local Standard of Rest (see, e.g., Mihalas & Binney 1981; Binney & Tremaine 2008), ICS = Integration Coordinate System for solar system bodies (see Section 4).

<sup>b</sup>For normally distributed velocities,  $\sigma$  = standard deviation;  $\sigma^2$  = variance.

<sup>c</sup>Sun’s “apex velocity” (depends on stellar type).

The exact timescale here matters, i.e., it makes a difference whether changes in orbital parameters due to flybys become significant over 50 or, say, 60 Myr. For example, a major climate event, called the Paleocene-Eocene Thermal Maximum (PETM) occurred 56 Myr ago and is widely considered the best analog for massive carbon release to the Earth system (e.g., Zachos et al. 2005). Earth’s orbital configuration 56 Myr ago is relevant for determining the exact age, chronology, and trigger of the PETM (Zeebe & Lourens 2019). Hence, passing stars could matter for understanding the PETM if the characteristic timescale of long-term flyby effects is 50 Myr, but not if the timescale is 60 Myr. Importantly, note however that the finding of the PETM’s onset coinciding with a maximum in Earth’s orbital eccentricity (trigger mechanism, see Zeebe & Lourens 2019) is primarily based on geologic data, and secondarily on astronomical calculations. Thus, including stellar encounters in astronomical models could potentially make a difference in the computations (although highly unlikely as we demonstrate here), but not in the data. Below we

show that including secondary effects such as a lunar contribution and  $J_2$  in solar system models (not considered by Kaib & Raymond 2024) is critical to accurately determine the timescale over which flyby perturbations become significant in planetary orbital parameters.

It should also be emphasized that the relationship between stellar flybys and orbital forcing on the one hand, and the relationship between orbital forcing and terrestrial climate change on the other, are two different and separate issues. The latter relationship involves a complex, non-linear transfer function as the climate system response is strongly non-linear. The climate response is

a separate problem and does not enter the framework for the present study (for further information, see, e.g., Zeebe & Kocken 2024). The present study solely focuses on the relationship between stellar flybys and orbital forcing, which can be adequately described using the tools presented in Sections 3 and 4.

### 1.1. Causality

As mentioned above, scenarios have been discussed in the literature in which the Sun-like star HD 7977 ( $m = 1.07 M_\odot$ ) passed relatively close to the solar system about 2.8 Myr ago (e.g., Bailer-Jones 2022). Kaib & Raymond (2024) suggested that such a passage (if exceptionally close) constitutes “an important driver of paleoclimate” before  $\sim 50$  Myr ago, specifically focusing on the PETM (Zeebe & Lourens 2019). Considering causality, the sequence of events begs the question, can a stellar close encounter at  $t = -2.8$  Myr affect the PETM at  $t = -56$  Myr? Of course not. However, it could potentially affect our understanding of the PETM. Consider a large ensemble of hypothetical histories (trajectories) of the solar system. When integrated starting from a point in the past toward the present, only those trajectories are valid that satisfy the present state ( $\mathbf{X}_i, \mathbf{V}_i$ ) of solar system bodies at  $t = 0$  compatible with present observations (for notation, see Table 1). Now select two of those trajectories. One without (standard model), the other with a recent close encounter. Both trajectories are equally valid, only they have different histories, i.e., they diverge at some point in the past

when looking at them from the present. For instance, as a result of solar system chaos, the trajectory including the close encounter would differ vastly from the standard model, say, beyond 80 Myr ago or so (e.g., Zeebe 2017). So the question is at what time in the past exactly do the trajectories diverge, and, would a different trajectory, for example, change previous conclusions about orbital eccentricity forcing of Earth’s climate at the PETM 56 Myr ago (Zeebe & Lourens 2019). In principle, it is straightforward to answer these questions because the physical laws involved are time-reversible, and, in practice, the numerical integrations are started in the present and the equations of motions are integrated backward in time with a negative timestep. Thus, we can simply explore the space of possible past trajectories through ensemble integrations starting with valid  $(\mathbf{X}_i, \mathbf{V}_i)$  at  $t = 0$  and include/exclude recent close encounters, a series of distant stellar flybys, etc. Importantly, it turns out that the decisive factor in properly answering the questions above is the complexity of the solar system model employed in the integrations.

## 2. IMPULSE

As an initial orientation for the effect of passing stars on the solar system (or strength of the stellar perturbation) one may consider the impulse ( $I$ ). It appears natural to assume that the perturbation should somehow scale with the stellar mass ( $M_*$ ) of the passing star and some inverse function of its speed ( $v$ ) and minimum passing distance ( $d$ ), aka impact parameter. Indeed, to first order and for long stellar passage times, the impulse per unit mass on the Sun may be approximated by (e.g., Oort 1950; Rickman 1976):

$$I = \frac{2GM_*}{vd}, \quad (1)$$

where  $G$  is the gravitational constant;  $I$  is in units of  $\text{m s}^{-1}$  (SI). To illustrate the effects of stellar mass and impact parameter on a solar system orbit, we use the parameter  $I/d$  (see Appendix A):

$$I/d = \frac{2GM_*}{vd^2}. \quad (2)$$

For example, an exceptionally close encounter with a star of one solar mass at  $d = 1,000$  au and  $v = 50 \text{ km s}^{-1}$  would generate an impulse gradient per unit mass of  $I/d \simeq 7,300 \text{ m s}^{-1} \text{ pc}^{-1}$  (see Fig. 1). Importantly, relative to an exceptionally close encounter, the average impulse gradient for the 1,800 randomly generated flybys shown in Fig. 1 is much smaller, i.e.,  $I/d = 0.42 \text{ m s}^{-1} \text{ pc}^{-1}$  (flybys after Heisler et al. 1987, see Section 3). Briefly, the vast majority of flybys are

weak. Note that 1,800 flybys is an estimated number of stars passing the solar system within 100 Myr.

Note also that the equations given here to illustrate impulse and impulse gradient are for scaling purposes only. For our flybys, the inner planets complete multiple orbits on the stellar flyby’s characteristic timescale. For this case, Spurzem et al. (2009) derive a scaling for the change in, e.g., eccentricity as  $\propto d^{-2}$  for hyperbolic flybys, which is the same scaling as the impulse gradient (Eq. (2)); for parabolic flybys, Spurzem et al. (2009) derive a scaling  $\propto d^{-3/2}$ . Importantly, however, the results of the present paper are numerical (see below) and the impulse scaling does not affect our results or conclusions; they are merely provided to motivate our results.

## 3. METHODS: FLYBYS

To generate random stellar flyby parameters, we tested three options. (1) Following the method and parameters from Heisler et al. (1987), (2) taking parameters from García-Sánchez et al. (2001), and (3) using the `airball` package (Brown et al. 2024).

### 3.1. Stellar Flybys following Heisler et al.

#### 3.1.1. Stellar type

Define a quantity  $S$ :

$$S = \sum_{i=1}^{20} n_i \sigma_i, \quad (3)$$

where  $n_i$  is the number density per  $\text{pc}^{-3}$  of stars of type  $i$  ( $N = 20$ ) and  $\sigma_i^2$  the variance of its velocity distribution ( $\sigma_i =$  dispersion in  $\text{km s}^{-1}$ , see Table 1 in Heisler et al. (1987)). Note that  $S$  is equivalent to a star flux (in SI units:  $1/(\text{m}^2\text{s})$ ). Cumulative and normalized, we can write:

$$S_k = \sum_{i=1}^k n_i \sigma_i / S, \quad (4)$$

where  $0 < S_k < 1$ . Thus, for a uniformly distributed random variable  $q$  ( $0 < q < 1$ ), Eq. (4) can be used to assign a stellar type with  $\sigma_i$  and mass  $m_i$ . The standard model of Heisler et al. (1987) gives a mean encounter rate  $f$  within  $r_{\text{max}} = 1 \text{ pc}$  of

$$f = \sqrt{8\pi} S r_{\text{max}}^2 = 13.15 \text{ Myr}^{-1}. \quad (5)$$

However, in our numerical simulations, stars were injected after certain time intervals with an average encounter rate of  $\sim 18 \text{ Myr}^{-1}$  (see Section 4.2). Note that  $r_{\text{max}} = 1 \text{ pc}$  was selected in the literature, for example, to include aphelion distances of most comets (Remy & Mignard 1985) but has also been adopted to study, for

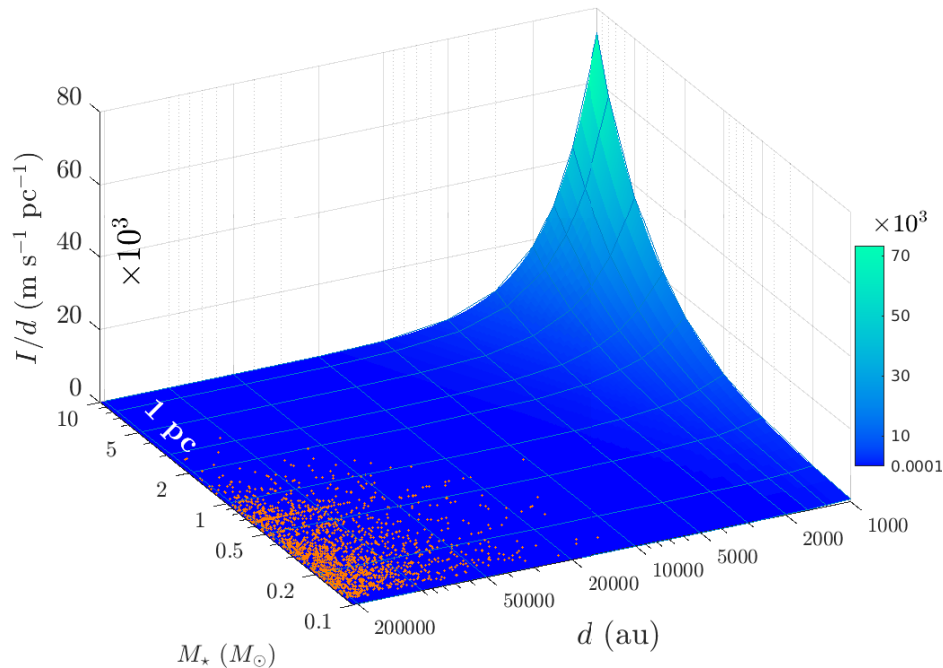


**Figure 1.** Illustration of impulse gradient per unit mass (Eq. (2)) for stellar flybys as a function of stellar mass ( $M_\star$ ) and minimum passing distance ( $d$ ). The upper  $d$  limit shown is 1 pc = 206,265 au (see Section 3.1). The colored surface uses a stellar speed  $v = 50 \text{ km s}^{-1}$ . Orange dots indicate example values for 1,800 flybys based on randomly generated stellar parameters (including  $v$ ) after Heisler et al. (1987), see Section 3; 1,800 flybys is an estimated number of stars passing the solar system within 100 Myr. The figure’s sole purpose is to illustrate the effect of different stellar parameters for very close, strong encounters (green-blue to green surface area) vs. average random flybys, which are weak (orange dots).

instance, impacts on planetary orbits (Kaib & Raymond 2024). We use the same value here for consistency. Furthermore, the impact of flybys on the solar system from encounters with  $d \gtrsim 1 \text{ pc}$  is relatively small (see Fig. 1).

### 3.1.2. Stellar injection coordinates

Consider a sphere of radius  $r_{\text{max}} = 1 \text{ pc}$  around the Sun centered at the origin  $[0,0,0]$  (coordinates here refer to the frame used in the numerical integrations, see Section 4). Stars were injected into the sphere at random positions  $\mathbf{r} = [x \ y \ z]$ , where  $x = r_{\text{max}} \sin \theta \cos \phi$ ,  $y = r_{\text{max}} \sin \theta \sin \phi$ ,  $z = r_{\text{max}} \cos \theta$ , with polar angle  $\theta$  ( $-1 < \cos \theta < +1$ ) and azimuth angle  $\phi$  ( $0 < \phi < 2\pi$ ), where  $\cos \theta$  and  $\phi$  are each uniformly and independently distributed. Note that for a random, isotropic distribution of  $\mathbf{r}$ , the  $z$  component is randomized (i.e.  $\cos \theta$ , not the angle  $\theta$  itself).

### 3.1.3. Stellar velocities

At each position  $\mathbf{r}$  on the sphere with radius  $r_{\text{max}}$ , stars were injected with velocity  $\mathbf{v} = [v_1 \ v_2 \ v_3]$ , where  $v_3$  is anti-parallel to  $\mathbf{r}$  and  $v_1, v_2$  perpendicular to  $v_3$ . The general assumption for the stellar velocity distribu-

tion is based on an isotropic Maxwell-Boltzmann distribution (e.g., Binney & Tremaine 2008; Tremaine 2023). Importantly, however, the velocity distribution for stars originating from a given area  $dA$  on the injection sphere is *not* isotropic (Hénon 1972).

The distribution function (or normalized pdf) for  $v_3$  and a given stellar type may be written as (Heisler et al. 1987):

$$f_3(v_3) = \frac{1}{\sigma^2} v_3 \exp(-v_3^2/2\sigma^2), \quad (6)$$

where  $f_3(v_3) \cdot dv_3$  is proportional to the probability of finding stars with velocities between  $v_3$  and  $v_3 + dv_3$ . To generate values for  $v_3$ , we sample the corresponding cdf:

$$F_3(v_3) = 1 - \exp(-v_3^2/2\sigma^2), \quad (7)$$

using a uniformly distributed random variable  $q$  ( $0 < q < 1$ ), i.e.,

$$v_3(q) = (-2\sigma^2 \ln(1 - q))^{\frac{1}{2}}. \quad (8)$$

The distribution function for  $v_1$  and  $v_2$  may be written as ( $i = 1, 2$ ):

$$f(v_i) = \left( \frac{1}{2\pi\sigma^2} \right)^{\frac{1}{2}} \exp(-v_i^2/2\sigma^2), \quad (9)$$

with cdf:

$$F_i(v_i) = \left[ 1 + \operatorname{erf}(v_i/\sqrt{2}\sigma) \right] / 2, \quad (10)$$

which we sample using uniformly distributed random variables  $q_i$ 's:

$$v_i(q_i) = \operatorname{erf}^{-1}(2q_i - 1) \cdot \sqrt{2}\sigma. \quad (11)$$

Once the stellar velocities  $\mathbf{v} = [v_1 \ v_2 \ v_3]$  have been determined in coordinates relative to  $\mathbf{r}$  (see above), they are transformed (rotated) into the solar system frame used in the numerical integrations (see Section 4).

### 3.1.4. The Sun's peculiar velocity

Heisler et al. (1987) did not take into account the Sun's peculiar velocity,  $\mathbf{v}_\odot$ , which we include here, loosely following Rickman et al. (2008). Once the stellar velocity vector  $\mathbf{v}$  (randomized directions), and its magnitude (speed)  $v$  has been obtained as described above (relative to the Local Standard of Rest), we modify  $\mathbf{v}$  to obtain the final stellar velocity (encounter velocity) as follows. We assume a random relative 3D orientation between the two vectors  $\mathbf{v}$  and  $\mathbf{v}_\odot$ , calculate the magnitude  $|\mathbf{v} - \mathbf{v}_\odot|$  and scale  $\mathbf{v}$  by that factor (for  $\mathbf{v}_\odot$  corresponding to each stellar type, see García-Sánchez et al. 2001; Rickman et al. 2008). For example, for typical  $v$  and  $v_\odot$  speeds of 40 and 23 km s<sup>-1</sup>, respectively, the procedure increases the final speed by about 4.4 km s<sup>-1</sup> on average for random  $\mathbf{v}$ - $\mathbf{v}_\odot$  orientations (see Appendix B).

### 3.2. Stellar Flybys using parameters from Garcia et al.

For the second option of generating random stellar flyby parameters, we used Heisler et al. (1987)'s methods but took the stellar parameters from García-Sánchez et al. (2001), see Table 8 and 1 in García-Sánchez et al. (2001) and Rickman et al. (2008), respectively. The velocity distribution is very similar to Heisler et al. (1987), in terms of dispersion  $\sigma$ , most probable, and mean speed  $\bar{v}$  (see Fig. 2). However, García-Sánchez et al. (2001) tends to yield larger stellar masses at somewhat higher frequency, mostly due to a generally higher number density  $n_i$  at a given mass.

### 3.3. Stellar Flybys using airball

For the third option, we used `airball` (a package for running and managing flybys, Brown et al. 2024) to generate parameters for our `orbitN` integrations. For the

stellar environment, we selected 'Local Neighborhood', a static environment representing the local neighborhood of the solar system. The velocity distribution is similar to Heisler et al. (1987) and García-Sánchez et al. (2001) (see Fig. 2). However, the `airball` environment generates larger stellar masses at lower frequency and appears not to include a significant population of white dwarfs (cf. mass peaks at 0.65 and 0.9  $M_\odot$ , Fig. 2 top and middle).

## 4. METHODS: SOLAR SYSTEM INTEGRATIONS

### 4.1. Basic integrator setup

Solar system integrations were performed following our earlier work (Zeebe 2015a,b, 2017) with the integrator package `orbitN` (Zeebe 2023a) using the symplectic integrator and Jacobi coordinates (Wisdom & Holman 1991; Zeebe 2015a). The simulations include contributions from general relativity, available as Post-Newtonian effects due to the dominant mass (Saha & Tremaine 1994). The Earth-Moon system was modeled as a gravitational quadrupole (Quinn et al. 1991) (`lunar` option), shown to be consistent with expensive Bulirsch-Stoer integrations (full dynamical separate Moon) up to 63 Ma (Zeebe 2017). Initial conditions for the positions and velocities of the planets and Pluto for ZB18a (reference astronomical solution) were generated from the DE431 ephemeris (Folkner et al. 2014) using the SPICE toolkit for Matlab. We had previously also tested the latest JPL ephemeris DE441 (Park et al. 2021), which makes little difference for practical applications because the divergence time relative to ZB18a (based on DE431) is  $\sim 66$  Ma and hence beyond ZB18a's reliability limit of  $\sim 58$  Ma (based on geologic data, see below). The integrations for ZB18a (timestep  $\Delta t = -2$  days, avoiding numerical chaos, see Hernandez et al. 2022) include 10 asteroids (Zeebe 2017), with initial conditions generated at [ssd.jpl.nasa.gov/x/spk.html](http://ssd.jpl.nasa.gov/x/spk.html). The asteroids were treated as heavyweight particles, subject to the same full interactions as the planets. Coordinates were obtained at JD2451545.0 in the ECLIPJ2000 reference frame and subsequently rotated to account for the solar quadrupole moment ( $J_2$ ) alignment with the solar rotation axis (Zeebe 2017). Earth's orbital eccentricity and inclination from ZB18a is available at [www2.hawaii.edu/~zeebe/Astro.html](http://www2.hawaii.edu/~zeebe/Astro.html) and [www.ncdc.noaa.gov/paleo/study/26970](http://www.ncdc.noaa.gov/paleo/study/26970). Importantly, we provide results from  $-100$  to  $0$  Myr but caution that the interval from  $-100$  to  $-58$  Myr is unconstrained due to dynamical chaos (Zeebe & Lourens 2019).

### 4.2. Ensemble integrations

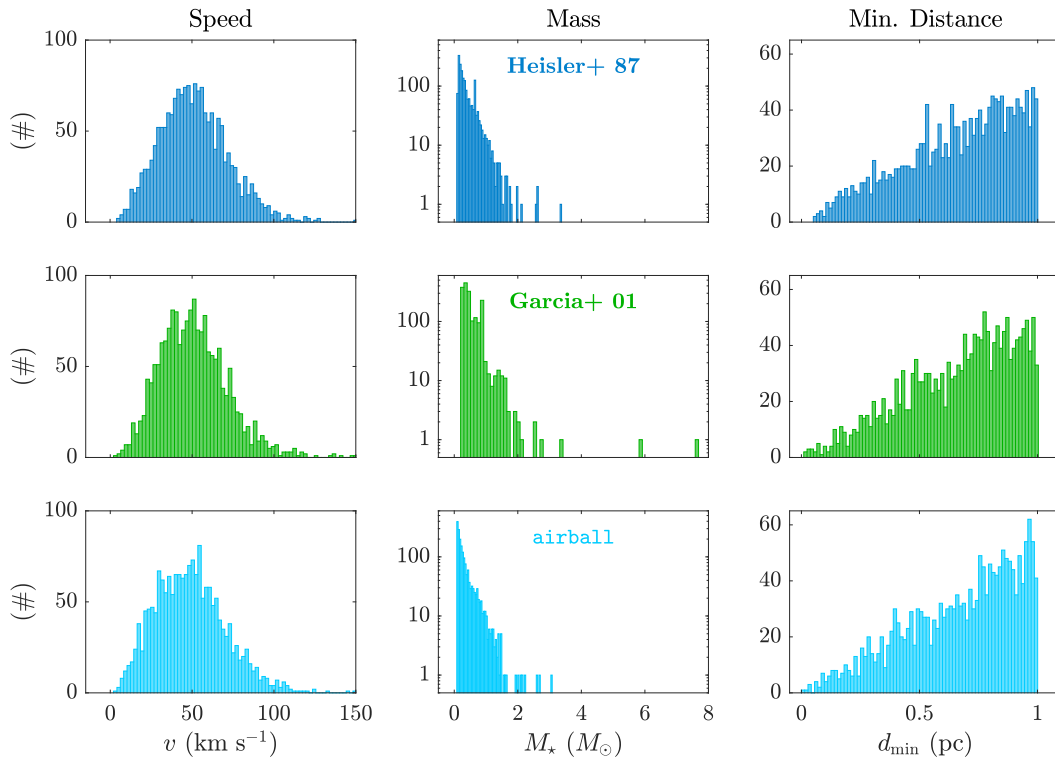


**Figure 2.** Random stellar flyby parameters generated following Heisler et al. (1987), García-Sánchez et al. (2001), and airball (top, middle, bottom row). Shown are example histograms for 1,800 flybys each. Note the logarithmic ordinate for mass. García-Sánchez et al. (2001) tends to yield larger stellar masses at somewhat higher frequency, mostly due to a generally higher number density  $n_i$  at a given mass (see text). The largest  $d_{\min}$  considered here is 1 pc, as stars are injected into a sphere around the Sun with  $r_{\max} = 1$  pc (see Section 3.1).

We generated 128 different sets of random stellar parameters for each of the three options described in Section 3. Each set was integrated in parallel on the high performance computing cluster Derecho (CISL 2023) for a total of  $N = 384$  ensemble simulations. All other integration parameters were held constant (Section 4.1). Stars were injected after roughly equal time intervals, yielding an average frequency of  $\sim 18$  passing stars per million years, consistent with Kaib & Raymond (2024). In addition, we generated one hypothetical solution  $S_{\text{HD7977}}$ , which includes randomly passing stars, as well as a (hypothetical) very close encounter with HD 7977 at  $t = -2.86$  Myr and  $d_{\min} = 3,896$  au (5% likelihood, see Bailer-Jones 2022).

## 5. RESULTS

### 5.1. Divergence time $\tau$ and HD 7977

The critical result of this study is the timescale over which solutions that include passing stars differ from our standard model, or reference solution ZB18a, which does not include passing stars. We determine that timescale by using  $\tau$ , the time when  $\max|\Delta e_{\oplus}|$  irreversibly crosses  $\sim 10\%$  of mean  $e_{\oplus}$ ;  $\tau$  is taken positive,

as defined in Zeebe (2017), see Fig. 3. Note that defining  $\tau$  when  $\max|\Delta e_{\oplus}|$  crosses a given threshold once would frequently result in  $\tau$ 's that are too short, because  $\max|\Delta e_{\oplus}|$  may drop again below the threshold beyond that time, where solutions show a good match (see Fig. 3 and Section 5.1.1). To avoid  $\tau$ 's that are too short, our criterion includes the qualifier “irreversibly”<sup>1</sup>. For  $t > -\tau$ , the solutions are practically indistinguishable and hence flybys do not affect our understanding of any events within the time interval  $[-\tau, 0]$ . For example, if  $\tau > 56$  Myr, our conclusions about orbital forcing of the PETM remain unchanged (Zeebe & Lourens 2019). For  $S_{\text{HD7977}}$ ,  $\tau \simeq 70$  Myr (Fig. 3) and thus even a hypothetical very close encounter at  $t = -2.86$  Myr and  $d_{\min} = 3,896$  au does not alter our understanding of the PETM.

#### 5.1.1. Geologically discernible differences

<sup>1</sup> Strictly, crossing the threshold is not an irreversible operation, but appears irreversible on the  $\sim \mathcal{O}(100)$  Myr time scale considered in this paper.

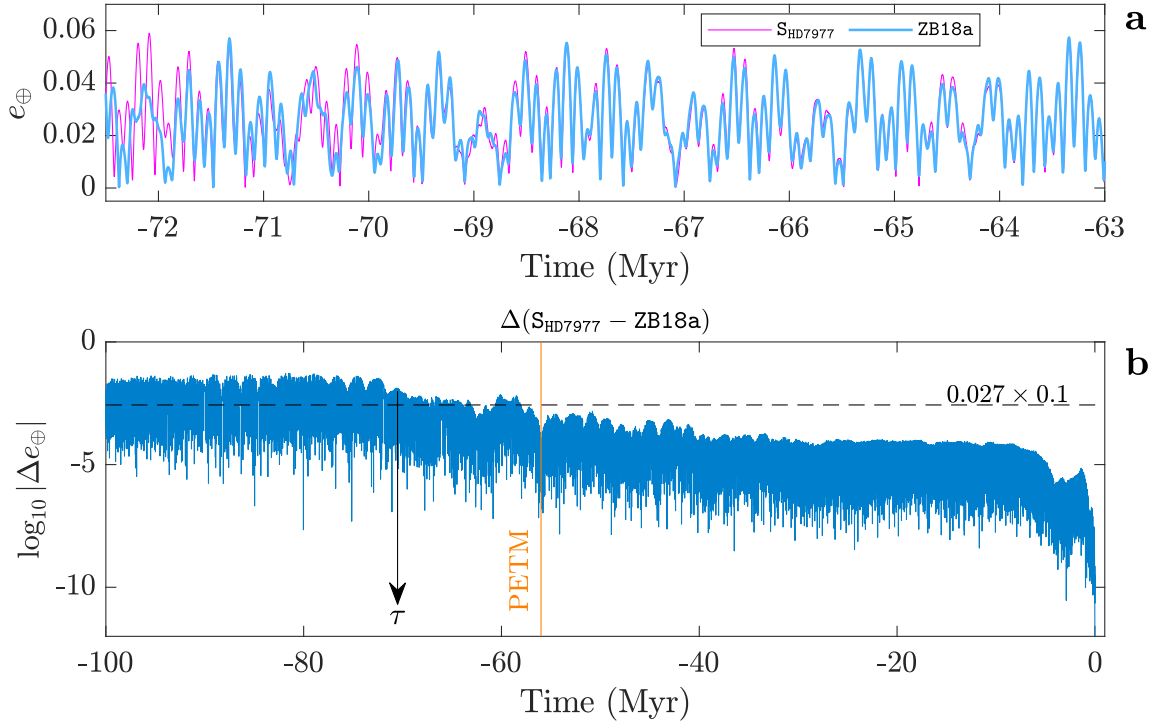


**Figure 3.** Example of divergence time  $\tau$ . (a) Earth’s orbital eccentricity,  $e_{\oplus}$ , for solutions  $S_{\text{HD7977}}$  and our standard model  $Z\text{B18a}$ . The setup for  $S_{\text{HD7977}}$  includes randomly passing stars, as well as a (hypothetical) very close encounter with HD 7977 ( $d_{\text{min}} = 3,896$  au,  $t = -2.86$  Myr). Notable differences between the two solutions appear around  $t = -70$  Myr. (b) Difference in Earth’s orbital eccentricity on a log-y scale,  $\log_{10} |\Delta e_{\oplus}|$ , between solutions  $S_{\text{HD7977}}$  and  $Z\text{B18a}$  over the past 100 Myr. The arrow indicates  $\tau \simeq 70$  Myr ( $\tau$  is taken positive), when  $\max|\Delta e_{\oplus}|$  irreversibly crosses  $\sim 10\%$  of mean  $e_{\oplus}$  ( $\sim 0.027 \times 0.1$ , dashed horizontal line). Importantly,  $\tau \simeq 70$  Myr is far beyond the PETM age ( $\sim 56$  Ma, vertical orange line).

The time at which the imprint of different  $e_{\oplus}$ ’s in a geologic archive would become discernible may slightly differ from  $\tau$ . Different  $e_{\oplus}$ ’s originate from different astronomical solutions and comparison with geological data ultimately allows distinguishing/selecting between the solutions (see Zeebe & Lourens 2019, 2022). Earth’s orbital eccentricity amplitude is modulated by the secular frequency term ( $g_4 - g_3$ ), which leads to so-called very long eccentricity nodes (VLNs) that can be detected in geologic archives (e.g., Zeebe & Lourens 2019; Zeebe & Kocken 2024). VLN intervals show a weak amplitude of the short-eccentricity cycle ( $\sim 100$ -kyr), with a recent period of  $\sim 2.4$  Myr. VLNs occur in  $Z\text{B18a}$ , for example, roughly around  $-72$ ,  $-70.5$ ,  $-69$  Myr, and so on (see Fig. 3a). In  $S_{\text{HD7977}}$ , VLNs also occur roughly around  $-70.5$  and  $-69$  Myr, but not around  $-72$  Myr, where its 100-kyr amplitude is strong (for amplitudes and VLNs, see Fig. 3a). In this case, the time to distinguish between  $Z\text{B18a}$  and  $S_{\text{HD7977}}$  based on geological data using VLNs would be ca.  $-72$  Myr, compared to ca.  $-70$  Myr based on  $\tau$ . Note that the small  $e_{\oplus}$  dif-

ferences for  $t > -70$  Myr (Fig. 3a) are unlikely to be detected in a geologic record.

## 5.2. Ensemble integrations

Of our 384 ensemble simulations, 383 show  $\tau > 56$  Myr (see Fig. 4), while a single solution ( $S_{80}$ ) shows  $\tau < 56$  Myr.  $S_{80}$  represents a simulation with a randomly generated (hypothetical), exceptional close encounter at  $t \simeq -1.2$  Myr,  $d_{\text{min}} \simeq 0.00339$  pc (699 au), and  $M_{\star} = 0.23 M_{\odot}$ . However, there is no evidence for such a close encounter in, for instance, Gaia DR3, for which Bailer-Jones (2022) found the G3 dwarf HD 7977 to be the closest encounter in the past. Thus, our ensemble simulations (Fig. 4), as well as our solution  $S_{\text{HD7977}}$  (Fig. 3), show that our understanding of the PETM, for instance, at  $t = -56$  Myr is not affected by stellar flybys.

We had previously shown that a reduced physical model which omits the lunar and  $J_2$  contributions leads to substantially shorter  $\tau$ ’s in solar system integrations (see Fig. 4 in Zeebe 2023a, reproduced in Fig. 4 here). These simulations did not include stellar flybys but dif-

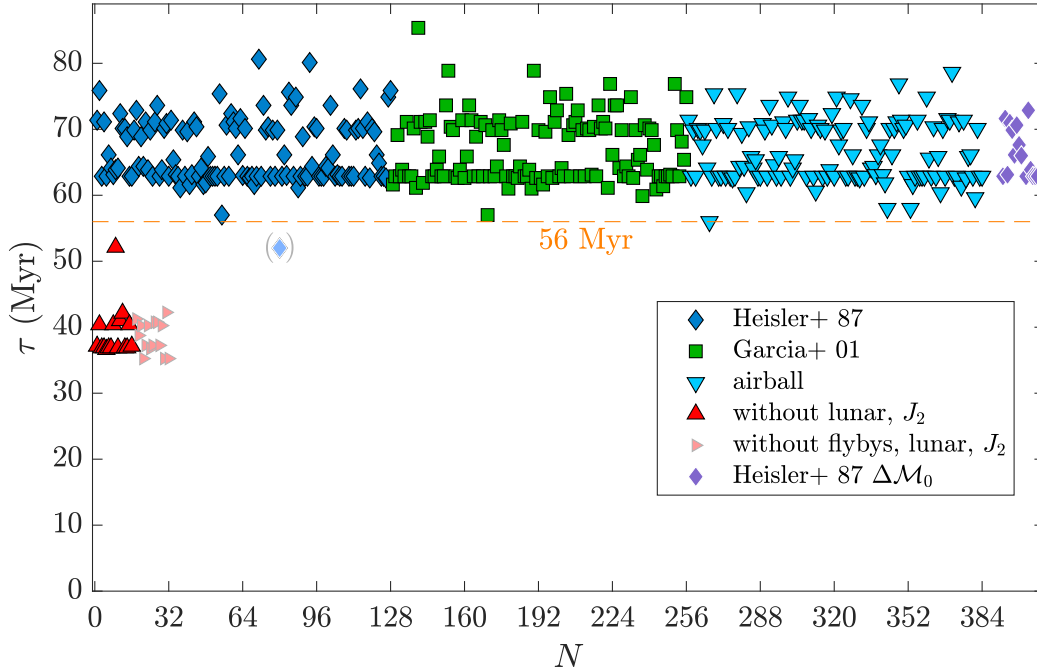


**Figure 4.** Divergence times,  $\tau$ 's, for ensemble runs ( $N = 3 \times 128$ , blue and green symbols) relative to our reference astronomical solution (standard model) ZB18a (see Fig. 3). Random stellar parameters for the three sets of 128 solutions are based on Heisler et al. (1987), García-Sánchez et al. (2001), and `airball`. All  $\tau \geq 56$  Myr, except for the symbol in parentheses ( $\tau < 56$  Myr), indicating one run (solution  $S_{80}$ ) with a randomly generated (hypothetical), exceptional close encounter at  $t \simeq -1.2$  Myr and  $d_{\min} \simeq 699$  au, for which there is no evidence in Gaia DR3 (see text and Bailer-Jones 2022). Also shown are  $\tau$ 's from runs including stellar flybys but omitting the lunar contribution and  $J_2$  (red triangles,  $\triangle$ ,  $N = 16$ ), resembling the approach of Kaib & Raymond (2024). Light red triangles ( $\triangleright$ ,  $N = 16$ ): no stellar flybys, no lunar contribution and  $J_2$ , but different initial positions for Earth (see Fig. 4 in Zeebe 2023a). Purple diamonds ( $N = 16$ ): first 16 ensemble runs repeated including random variations in the initial mean anomaly  $\mathcal{M}_0$  of each body (see Section 5.3). For more information on  $\tau$  and solar system chaos, see Zeebe (2023a) and Zeebe & Kocken (2024).

ferent initial positions for Earth. For the present study, we ran 16 additional simulations including stellar flybys and omitting the lunar and  $J_2$  contributions, which resembles the approach of Kaib & Raymond (2024). The results show that regardless of whether initial conditions are modified or flybys are included, a reduced physical model that ignores the lunar contribution and  $J_2$  enhances long-term instability and leads to substantially shorter  $\tau$ 's (see Fig. 4). All of our simulations use an accurate and fast implementation of general relativity (GR), i.e., Post-Newtonian effects due to the dominant mass, following Saha & Tremaine (1994). In contrast, Kaib & Raymond (2024) used a simplified central force modification to induce GR precession (potential  $\propto 1/(c^2 r^2)$ ). However, given that our results for all  $\tau$ 's (with and without lunar and solar quadrupole) were obtained with the same GR implementation suggests that the GR model is of minor importance in this particular instance.

The small  $\tau$  for solution  $S_{80}$  with an exceptional close encounter may suggest a general relationship between  $\tau$  and the strength of the flyby. However, dynamical chaos imposes at least two restrictions on such a relationship. First, there is a characteristic timescale over which flyby perturbations become significant in planetary orbital parameters, i.e., around 50 to 60 Myr for the average flyby strength considered here (see Section 1). Thus, for a flyby solution to show significant differences to the standard model, say at  $t = -50$  Myr, the encounter has to occur close to the present (for a discussion of causality, see Section 1.1). Second, the exact long-term evolution of small perturbations is not predictable in detail due to chaos and often appears random (see Zeebe 2023a). Thus, a correlation between  $\tau$  and the flyby strength is only expected for strong encounters. Note that our  $\tau$  measures differences across a 50-Myr timescale, which is different from a 1-Myr timescale (see Fig. 3 in Kaib & Raymond 2024). For strong encounters with impulse

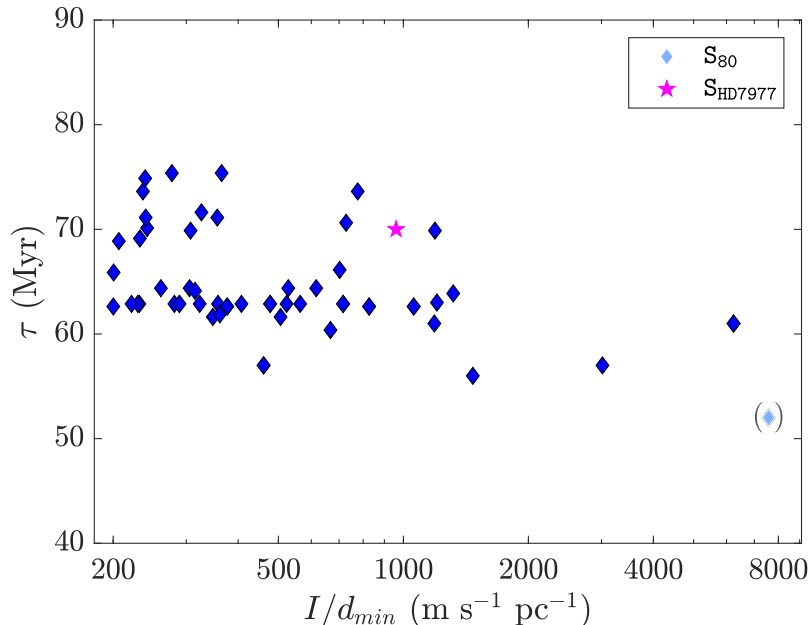


**Figure 5.** Divergence times,  $\tau$ 's, vs. impulse gradient ( $I/d_{\min}$ ) shown for runs with strong close encounters  $I/d_{\min} > 200 \text{ m s}^{-1} \text{ pc}^{-1}$  that occur within the time interval  $[-20 \text{ } 0] \text{ Myr}$ . Note that flybys with  $I/d_{\min} \ll 200 \text{ m s}^{-1} \text{ pc}^{-1}$  are very frequent (multiple per run) and exhibit no relationship with  $\tau$  at all (not shown, see text). Also note the logarithmic abscissa.

gradients  $I/d_{\min} > 200 \text{ m s}^{-1} \text{ pc}^{-1}$  that occur within the time interval  $[-20 \text{ } 0] \text{ Myr}$ , a weak relationship between  $\tau$  and  $I/d_{\min}$  appears to be present (see Fig. 5). For example, the smallest  $\tau$  is indeed associated with the largest flyby impulse gradient (solution  $\mathcal{S}_{80}$ ). However, for the vast majority of flybys (which are weak), the impulse gradient is in general a poor predictor for  $\tau$ , whose variability is dominated by dynamical chaos.

### 5.3. Randomized initial conditions

In order to explore the possible parameter space of orbital solutions resulting from dynamical chaos, randomized initial conditions (unique to each solution) have been used in the past (e.g., Laskar et al. 2011; Zeebe 2015b). For otherwise identical integrations, unique sets of initial conditions ensure that no two ensemble members are alike. Importantly, however, in the present case the integrations are *not* identical because of different sets of random stellar parameters generated for each ensemble member, resulting indeed in 384 unique solutions (see Fig. 4). Kaib & Raymond (2024) varied the initial mean anomaly ( $\mathcal{M}_0$ ) of each body at  $t_0$  by a random amount, generating an orbital shift between  $\pm 2 \text{ cm}$  (ca.  $\pm 1.3 \times 10^{-13} \text{ au}$ ). However, the magnitude of the perturbation due to a typical stellar flyby (1,800 of which occur throughout the simulation, including close to  $t_0$ )

is much larger. Thus, randomizing the initial conditions for the current ensemble runs is unnecessary.

Nevertheless, to demonstrate the effect of random flybys vs. random initial conditions, we repeated the first 16 runs of our ensemble simulations (following Heisler et al. 1987), as well as  $\mathcal{S}_{80}$ , with small modifications. Note that  $\mathcal{S}_{80}$  includes a randomly generated (hypothetical), exceptional close encounter at  $t \simeq -1.2 \text{ Myr}$ . Relative to the reference initial conditions of ZB18a,  $\mathcal{M}_0$  of each body (including asteroids) at  $t_0$  was randomized, resulting in small offsets within  $\pm 2 \text{ cm}$ . The results show that  $\Delta \mathcal{M}_0$  has no systematic effect on  $\tau$  (all  $\tau$ 's  $> 60 \text{ Myr}$ , Fig. 4, purple diamonds). The reduced  $\tau$ 's (Fig. 4, red triangles) are due to reduced physics, not initial conditions. The modified and original  $\mathcal{S}_{80}$  runs yielded identical  $\tau$ 's (although the simulations themselves were not identical).

## 6. CONCLUSIONS

In contrast to Kaib & Raymond (2024), we find no influence of passing stars on paleoclimate reconstructions over the past 56 Myr. The reason for the contrasting results is the simplified solar system model employed by Kaib & Raymond (2024), which omits the Moon (or any lunar contribution) and  $J_2$ . Notably, it has been demonstrated previously that both the lunar contribu-

tion and  $J_2$  have a stabilizing effect, i.e., extend the divergence time  $\tau$ , on a 100 Myr timescale (see Fig. 4 in Zeebe (2023a)), which is confirmed here. In order to draw accurate conclusions about the solar system’s stability and chaotic behavior on a 100 Myr timescale, full state-of-the-art models need to be employed that consider all known secondary effects, including general relativity, a lunar contribution,  $J_2$ , and asteroids (Zeebe 2023a; Zeebe & Kocken 2025).

Briefly, the reason for, e.g., the lunar contribution to have a stabilizing effect (extending  $\tau$ ) is its long-term effect on secular frequencies, specifically involving the secular resonance  $m(g_4 - g_3) - (s_4 - s_3)$ , where  $m = 1, 2$ . Full state-of-the-art solar system models show a resonance transition from  $m = 1$  to  $m = 2$  around  $t = -50$  Myr (e.g., Laskar et al. 2011; Zeebe & Lourens 2019, 2022). Omitting the lunar contribution tends to shift the timing of the resonance transition toward the present, thereby making the system less stable and shortening  $\tau$ . The details are complex, however (see discussions in Zeebe 2023a; Zeebe & Kocken 2025) and deserve a proper, separate analysis, which is beyond the scope of this paper.

Running accurate state-of-the-art solar system models that include all known secondary effects is computationally expensive. As a result, long-term studies on, e.g., Gyr-timescale tend to be based on simplified solar system models, or the outer planets alone (e.g., Zink et al. 2020; Brown & Rein 2022). One question to be addressed in future work is whether or not the results of such studies would be significantly different using more complete solar system models.

**Acknowledgments.** This research was supported by Heising-Simons Foundation Grants #2021-2800 and #2021-2803 (R.E.Z. and D.H.M) and U.S. NSF grant OCE20-34660 to R.E.Z. We thank the reviewers for suggestions, which improved the manuscript.

*Software:* `orbitN`, [github.com/rezeebe/orbitN](https://github.com/rezeebe/orbitN); on Zenodo: [zenodo.org/records/8021040](https://zenodo.org/records/8021040), Zeebe (2023b).

## APPENDIX

### A. IMPULSE SCALING

For the effect of a passing star on a comet, Rickman (1976) derived an equation for the impulse per unit mass:

$$I' = \frac{2GM_\star}{vd^2} \cdot r_c \sin \alpha, \quad (\text{A1})$$

where  $r_c = |\mathbf{r}_c|$  is the comet’s typical distance from the sun ( $\mathbf{r}_c =$  heliocentric position vector) and  $\alpha$  the angle between the vector pointing from the sun to the passing star and the plane perpendicular to  $\mathbf{r}_c$  (see Fig. 3 in Rickman 1976). For small eccentricities,  $r_c$  may be replaced by the semimajor axis  $a$ . Furthermore, for a given  $a$  and flyby geometry (which sets  $\alpha$ ),  $I'$  scales with:

$$\frac{2GM_\star}{vd^2} = I/d, \quad (\text{A2})$$

where  $I$  is given by Eq. (1). We use  $I/d$  for illustration in Fig. 1 and for the relationship between strong encounters and  $\tau$  in Fig. 5. The parameter  $2GM_\star/(vd^2)$  corresponds to Kaib & Raymond (2024)’s impulse gradient.

### B. PECULIAR VELOCITY CONTRIBUTION

In the following, we estimate the average peculiar velocity contribution for random orientations relative to the stellar velocity. Let us denote the stellar velocity as  $\mathbf{v} = [v_1 \ v_2 \ v_3]$ , and the Sun’s peculiar velocity here as  $\mathbf{v}_\odot = \mathbf{u} = [u_1 \ u_2 \ u_3]$ ;  $|\mathbf{u}| = u$ . The final encounter speed is:

$$v_f = [(v_1 - u_1)^2 + (v_2 - u_2)^2 + (v_3 - u_3)^2]^{\frac{1}{2}}. \quad (\text{B3})$$

Without loss of generality, select a coordinate system in which  $\mathbf{v} = [0 \ 0 \ v_3]$  and the transformed  $v_3 > 0$ ;  $|\mathbf{v}| = v_3$ . Also, use spherical coordinates for  $\mathbf{u}$ :

$$v_f = [(u \sin \theta \cos \phi)^2 + (u \sin \theta \sin \phi)^2 + (v_3 - u \cos \theta)^2]^{\frac{1}{2}}. \quad (\text{B4})$$

Furthermore,  $u^2 \sin^2 \theta \cos^2 \phi + u^2 \sin^2 \theta \sin^2 \phi + u^2 \cos^2 \theta = u^2$ , and hence:

$$v_f = (v_3^2 + u^2 - 2v_3u \cos \theta)^{\frac{1}{2}}, \quad (\text{B5})$$

with maximum and minimum values of  $v_f = v_3 \pm u$ . To calculate an average  $v_f$  for random relative orientations, use  $\zeta = \cos \theta$  as variable (see Section 3.1.2 for isotropy) and integrate:

$$\overline{v_f} = \frac{1}{2} \int_{-1}^1 (v_3^2 + u^2 - 2v_3u \zeta)^{\frac{1}{2}} d\zeta. \quad (\text{B6})$$

Using  $a = v_3^2 + u^2$  and  $b = 2v_3u$ , integration yields:

$$\overline{v_f} = -\frac{1}{2} \cdot \frac{2}{3b} \left[ (a - b \zeta)^{\frac{3}{2}} \right]_{-1}^1. \quad (\text{B7})$$

For example, for typical  $v$  and  $u$  of 40 and 23 km s<sup>-1</sup>, respectively,  $v_f = 44.4$  km s<sup>-1</sup>, i.e., the final speed increases by about 4.4 km s<sup>-1</sup> on average.

### C. JUSTIFYING WISDOM–HOLMAN

`orbitN` utilizes the Wisdom–Holman method (WH), first introduced in Wisdom & Holman (1991). We demonstrate that the assumptions of this method hold even for extreme hyperbolic flybys considered in this paper. WH functions by splitting the orbital Hamiltonian ( $H$ ) into a dominant piece described by Keplerian conic sections, including hyperbolic orbits, and a perturbation to this motion. Expressed in equations,  $H = A + B$ , where  $|B|/|A| = \mathcal{O}(\epsilon)$ , and  $\epsilon \ll 1$  can be taken as the ratio of Jupiter’s mass to the solar mass ( $= 10^{-3}$ ) in the case of solar system studies. Compared to a usual solar system integration, the flyby introduces new terms into  $B$ , say  $B_F$ , and we need to check that,

$$|B_F|/|A| \leq \mathcal{O}(\epsilon). \quad (\text{C8})$$

The flyby also introduces new terms into  $A$ , say  $A_F$ . A reasonable assumption is that  $|A_F| \geq |A|$ , and so we can ignore  $A_F$  in what follows. Using notation from Hernandez & Dehnen (2017), we have,

$$B_F = \frac{Gm_0M_\star}{u_f} - \frac{Gm_0M_\star}{r_{0f}} - \sum_{0 < i < f} \frac{Gm_iM_\star}{r_{if}}. \quad (\text{C9})$$

Here,  $\mathbf{u}$  refers to Jacobi coordinates and  $f$  is the flyby index,  $m_0$  is the solar mass, and  $r_{if}$  is the separation of star and body  $i$ . Indices  $0 < i < f$  refer to the planetary and asteroidal masses. Eq. (C8) holds if  $\mathcal{O}(M_\star/r_{0f}) \leq \mathcal{O}(m_J/r_{0J})$ , with  $J$  the index of Jupiter and  $m_J/r_{0J} \simeq 2 \times 10^{-4}$  au<sup>-1</sup>. For example, for the strongest non-hypothetical flyby (HD 7977, 5% likelihood) we have  $M_\star = 1.07 m_0$  and  $r_{0f} = 3,900$  au, and hence  $M_\star/r_{0f} = 2.7 \times 10^{-4}$  au<sup>-1</sup>. For these values, we see,  $\mathcal{O}(M_\star/r_{0f}) = \mathcal{O}(m_J/r_{0J})$ , justifying our use of WH.

### REFERENCES

- Bailer-Jones, C. A. L. 2022, *ApJL*, 935, L9,  
doi: [10.3847/2041-8213/ac816a](https://doi.org/10.3847/2041-8213/ac816a)
- Batygin, K., Adams, F. C., Batygin, Y. K., & Petigura,  
E. A. 2020, *Astron. J.*, 159, 101,  
doi: [10.3847/1538-3881/ab665d](https://doi.org/10.3847/1538-3881/ab665d)
- Binney, J., & Tremaine, S. 2008, *Galactic Dynamics:*  
Second Edition (Princeton University Press)
- Bobylev, V. V., & Bajkova, A. T. 2022, *Astron. Lett.*, 48,  
542, doi: [10.1134/S1063773722080011](https://doi.org/10.1134/S1063773722080011)
- Brown, G., & Rein, H. 2022, *MNRAS*, 515, 5942,  
doi: [10.1093/mnras/stac1763](https://doi.org/10.1093/mnras/stac1763)
- Brown, G., Rein, H., Mohsin, H., et al. 2024, *Airball: a  
package for running and managing flybys using rebound.*  
[airball.readthedocs.io](https://airball.readthedocs.io)
- CISL. 2023, Computational and Information Systems  
Laboratory. Derecho: HPE Cray EX System (NCAR  
Community Computing), National Center for  
Atmospheric Research, Boulder, CO,  
doi: [doi:10.5065/qx9a-pg09](https://doi.org/10.5065/qx9a-pg09)
- de la Fuente Marcos, R., & de la Fuente Marcos, C. 2022,  
*Res. Notes AAS*, 6, 152, doi: [10.3847/2515-5172/ac842b](https://doi.org/10.3847/2515-5172/ac842b)

- Dybczyński, P. A., Królikowska, M., Bartczak, P., et al. 2024, *Astron. Astrophys.*, 685, A171, doi: [10.1051/0004-6361/202348995](https://doi.org/10.1051/0004-6361/202348995)
- Folkner, W. M., Williams, J. G., Boggs, D. H., Park, R. S., & Kuchynka, P. 2014, *Interplanetary Network Progress Report*, 196, 1
- García-Sánchez, J., Weissman, P. R., Preston, R. A., et al. 2001, *Astron. Astrophys.*, 379, 634, doi: [10.1051/0004-6361:20011330](https://doi.org/10.1051/0004-6361:20011330)
- Heisler, J., Tremaine, S., & Alcock, C. 1987, *Icarus*, 70, 269, doi: [10.1016/0019-1035\(87\)90135-7](https://doi.org/10.1016/0019-1035(87)90135-7)
- Hénon, M. 1972, *Astron. Astrophys.*, 19, 488
- Hernandez, D. M., & Dehnen, W. 2017, *MNRAS*, 468, 2614, doi: [10.1093/mnras/stx547](https://doi.org/10.1093/mnras/stx547)
- Hernandez, D. M., Zeebe, R. E., & Hadden, S. 2022, *MNRAS*, 510, 4302, doi: [10.1093/mnras/stab3664](https://doi.org/10.1093/mnras/stab3664)
- Kaib, N. A., & Raymond, S. N. 2024, *ApJL*, 962, L28, doi: [10.3847/2041-8213/ad24fb](https://doi.org/10.3847/2041-8213/ad24fb)
- Laskar, J., Fienga, A., Gastineau, M., & Manche, H. 2011, *Astron. Astrophys.*, 532, A89, doi: [10.1051/0004-6361/201116836](https://doi.org/10.1051/0004-6361/201116836)
- Laughlin, G., & Adams, F. C. 2000, *Icarus*, 145, 614, doi: [10.1006/icar.2000.6355](https://doi.org/10.1006/icar.2000.6355)
- Li, G., & Adams, F. C. 2015, *MNRAS*, 448, 344, doi: [10.1093/mnras/stv012](https://doi.org/10.1093/mnras/stv012)
- Malmberg, D., Davies, M. B., & Heggie, D. C. 2011, *MNRAS*, 411, 859, doi: [10.1111/j.1365-2966.2010.17730.x](https://doi.org/10.1111/j.1365-2966.2010.17730.x)
- Mihalas, D., & Binney, J. 1981, *Galactic astronomy. Structure and kinematics* (W. H. Freeman & Co.)
- Oort, J. H. 1950, *Bull. Astron. Inst. Neth.*, 11, 91
- Park, R. S., Folkner, W. M., Williams, J. G., & Boggs, D. H. 2021, *Astron. J.*, 161, 105, doi: [10.3847/1538-3881/abd414](https://doi.org/10.3847/1538-3881/abd414)
- Pfalzner, S., Govind, A., & Portegies Zwart, S. 2024, *Nat. Astron.*, 8, 1380, doi: [10.1038/s41550-024-02349-x](https://doi.org/10.1038/s41550-024-02349-x)
- Potemine, I. Y. 2024. <https://arxiv.org/abs/2402.13015>
- Quinn, T. R., Tremaine, S., & Duncan, M. 1991, *Astron. J.*, 101, 2287, doi: [10.1086/115850](https://doi.org/10.1086/115850)
- Remy, F., & Mignard, F. 1985, *Icarus*, 63, 1, doi: [10.1016/0019-1035\(85\)90016-8](https://doi.org/10.1016/0019-1035(85)90016-8)
- Rickman, H. 1976, *Bull. Astron. Inst. Czech.*, 27, 92
- Rickman, H., Fouchard, M., Froeschlé, C., & Valsecchi, G. B. 2008, *Celest. Mech. Dyn. Astron.*, 102, 111, doi: [10.1007/s10569-008-9140-y](https://doi.org/10.1007/s10569-008-9140-y)
- Saha, P., & Tremaine, S. 1994, *Astron. J.*, 108, 1962, doi: [10.1086/117210](https://doi.org/10.1086/117210)
- Spurzem, R., Giersz, M., Heggie, D. C., & Lin, D. N. C. 2009, *Astrophys. J.*, 697, 458, doi: [10.1088/0004-637X/697/1/458](https://doi.org/10.1088/0004-637X/697/1/458)
- Tremaine, S. 2023, *Dynamics of Planetary Systems* (Princeton University Press)
- Wisdom, J., & Holman, M. 1991, *Astron. J.*, 102, 1528, doi: [10.1086/115978](https://doi.org/10.1086/115978)
- Zachos, J. C., Röhl, U., Schellenberg, S. A., et al. 2005, *Science*, 308, 1611
- Zeebe, R. E. 2015a, *Astrophys. J.*, 798, 8, doi: [10.1088/0004-637X/798/1/8](https://doi.org/10.1088/0004-637X/798/1/8)
- Zeebe, R. E. 2015b, *Astrophys. J.*, 811, 9, doi: [10.1088/0004-637X/811/1/9](https://doi.org/10.1088/0004-637X/811/1/9)
- Zeebe, R. E. 2017, *Astron. J.*, 154, 193, doi: [10.3847/1538-3881/aa8cce](https://doi.org/10.3847/1538-3881/aa8cce)
- Zeebe, R. E. 2023a, *Astron. J.*, 166, doi: [10.3847/1538-3881/acd63b](https://doi.org/10.3847/1538-3881/acd63b)
- . 2023b, *orbitN: A Symplectic integrator for near-Keplerian planetary systems*, Zenodo, doi: [10.5281/ZENODO.8021040](https://doi.org/10.5281/ZENODO.8021040)
- Zeebe, R. E., & Kocken, I. J. 2024, *Earth-Sci. Rev.*, 104959, doi: [10.1016/j.earscirev.2024.104959](https://doi.org/10.1016/j.earscirev.2024.104959)
- . 2025, *Astron. J.*, accepted. <https://arxiv.org/abs/2505.00187>
- Zeebe, R. E., & Lourens, L. J. 2019, *Science*, 365, 926
- . 2022, *Earth Planet. Sci. Lett.*, 592, 117595, doi: [10.1016/j.epsl.2022.117595](https://doi.org/10.1016/j.epsl.2022.117595)
- Zink, J. K., Batygin, K., & Adams, F. C. 2020, *Astron. J.*, 160, 232, doi: [10.3847/1538-3881/abb8de](https://doi.org/10.3847/1538-3881/abb8de)